Lifetime of the surface magnetoplasmons in metallic nanoparticles

Guillaume Weick and Dietmar Weinmann

*Institut de Physique et Chimie des Matériaux de Strasbourg (UMR 7504), CNRS, and Université de Strasbourg, 23 rue du Loess,
BP 43, F-67034 Strasbourg Cedex 2, France*

We study the influence of an external magnetic field on the collective electronic excitations in metallic nanoparticles. While the usual surface plasmon corresponding to the collective oscillation of the electrons with respect to the ionic background persists in the direction parallel to the magnetic field, the components in the perpendicular plane are affected by the field and give rise to two collective modes with field-dependent frequencies, the surface magnetoplasmons. We analyze the decay of these collective excitations by their coupling to particle-hole excitations and determine how their lifetimes are modified by the magnetic field. In particular, we show that the lifetime of the usual surface plasmon is not modified by the magnetic field, while the lifetime of the two surface magnetoplasmons present a weak magnetic-field dependence. Optical spectroscopy experiments are suggested in which signatures of the surface magnetoplasmons may be observed.

PACS number(s): 73.20.Mf, 73.22.Lp, 78.67.Bf

I. INTRODUCTION

Collective excitations in confined many-body systems are of great fundamental interest. Such excitations decay due to their coupling to other internal degrees of freedom of the system. This allows the study of quantum dissipation and decoherence and thereby the transition between quantum and classical physics. Particularly well studied is the case of surface plasmon excitations in metallic nanoparticles.[1–4] These collective dipolar vibrations of the electronic center of mass with respect to the ionic background dominate the optical absorption spectrum. The corresponding resonance linewidth gives indirect access to the lifetime of the surface plasmon. Moreover, pump-probe experiments allow one to follow the time evolution of the electron dynamics with a resolution of a few femtoseconds,[5–7] and the surface plasmon excited by the probe laser field plays a prominent role in the interpretation of the pump-probe measurements.[8] Recently, this technique was combined with magneto-optical Kerr effect measurements to follow the magnetization dynamics in superparamagnetic transition-metal nanoparticles and in particular the ultrafast demagnetization resulting from the pump laser excitation.[9] This demagnetization is also observed in ferromagnetic thin films,[10] and its explanation is still a matter of debate.[11,12]

The saturation magnetization in ferromagnetic materials plays the role of an effective *external* magnetic field that couples to the orbital degrees of freedom.[13] It is therefore relevant to study the influence of this effective field on the collective resonances in nanoparticles. In this work, we focus on the generic problem of the role played by an external magnetic field on the collective resonances in spherical *nonmagnetic* (i.e., alkaline or noble-metal) nanoparticles. While the surface plasmon excitation with the dipole parallel to the magnetic field is not modified, the two plasmon modes with dipoles perpendicular to the field evolve in two magnetic-field-dependent collective modes when the magnetic field is switched on (see Fig. 1). We term these collective excitations "surface magnetoplasmons." They are split in energy by an amount of the order of the cyclotron frequency ω_c. Similar excitations exist in quasi-two-dimensional semiconductor

quantum dots.[14,15] In the case of quantum dots, the energy scale of the resonance energies is not in the optical but in the infrared range, and the coupling of the collective excitation to the other degrees of freedom is very weak.[16,17] In contrast, in metallic nanoparticles, this coupling is quite strong and leads to the decay of the collective modes. It is the aim of the present paper to analyze in detail the consequences of such a coupling on the lifetime of the surface magnetoplasmons. As we show in the sequel, the coupling yields a non-negligible linewidth of the corresponding resonances which might limit their observability in experiments.

In this work, we analyze the decay of the surface magnetoplasmons in metallic nanoparticles which is caused by their coupling to particle-hole excitations. This process, called Landau damping,[3] is the dominant decay channel for intermediate-size nanoparticles with a radius a in the range 1 nm $\lesssim a \lesssim$ 10 nm.[18] We show that the surface magnetoplasmon lifetimes (whose inverses yield the linewidths of the resonances) increase linearly with the size of the nanoparticle, as it is the case for the well-studied surface plasmon lifetime.[4,19–24] For experimentally available magnetic
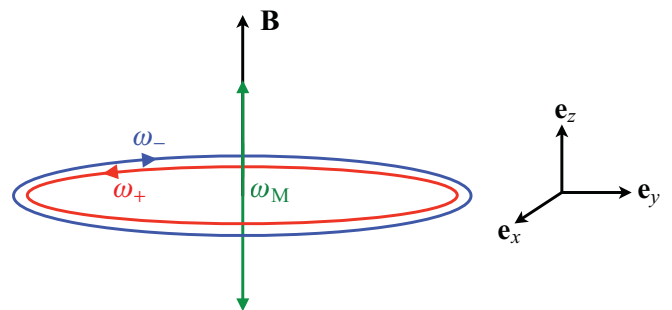

FIG. 1. (Color online) Sketch of the center-of-mass motion with frequency ω_M for the surface plasmon collective mode parallel to the magnetic field **B** and for the two surface magnetoplasmon modes with frequencies ω_+ and ω_- [cf. Eq. (17)], where it rotates counterclockwise and clockwise in the plane perpendicular to **B**, respectively.

fields, the surface magnetoplasmon linewidths are of the same order as the linewidth γ of the usual surface plasmon. Since typically $\omega_c \ll \gamma$, it is very difficult to individually resolve the collective magnetoplasmon resonances in a direct absorption experiment. However, we propose an indirect way to detect the predicted magnetic-field-induced modification of the absorption spectrum by means of optical spectroscopy experiments. When the electric field of the exciting laser is linearly polarized parallel to the external magnetic field, only the usual surface plasmon is triggered. In contrast, when the electric field is perpendicular to the external magnetic field, only the surface magnetoplasmons are excited (see Fig. 1). Using circularly polarized light, the two surface magnetoplasmon modes can be individually addressed. The difference in the resulting absorption spectra should be clearly detectable with experimentally available magnetic fields.

Furthermore, we argue that our results should be applicable, at least qualitatively, for ferro- or superparamagnetic nanoparticles, where the saturation magnetization is similar to an effective external magnetic field.[13] It might therefore be necessary to include the effect of the magnetic field on the electronic center-of-mass motion when one attempts to model the effect of laser light on the magnetization of such nanoparticles.

The paper is organized as follows: In Sec. II, we present our model and the relevant collective coordinates to describe the surface magnetoplasmon dynamics. We calculate their lifetimes, which constitute the main result of the present paper, in Sec. III. We suggest in Sec. IV optical absorption spectroscopy experiments to observe the surface magnetoplasmon collective modes before we conclude in Sec. V. Several technical issues are explained in the appendices.

II. MICROSCOPIC MODELING OF SURFACE MAGNETOPLASMONS

We consider a spherical nanoparticle in vacuum containing N valence electrons of charge $-e$ and mass m_e. The nanoparticle of radius $a = r_s N^{1/3}$ with $r_s = (3/4\pi n_e)^{1/3}$, the Wigner-Seitz radius (n_e is the electronic density), is subject to a homogeneous magnetic field $\mathbf{B} = \nabla \times \mathbf{A}$, where $\mathbf{A}$ is the vector potential. Within the jellium approximation, which assumes a homogeneous positive background of charge $+Ne$ (Ref. 2), the electronic Hamiltonian reads[25]

$$H = \sum_{i=1}^{N} \left[\frac{1}{2m_e}\left(\mathbf{p}_i + \frac{e}{c}\mathbf{A}(\mathbf{r}_i) \right)^2 + U(r_i) + \frac{g_e \mu_B}{\hbar}\mathbf{B} \cdot \mathbf{s}_i \right]$$
$$+ \sum_{i,j=1(i \neq j)}^{N} \frac{e^2}{2|\mathbf{r}_i - \mathbf{r}_j|}, \qquad (1)$$

where $g_e \simeq 2$ is the electronic g factor, $\mu_B = e\hbar/2m_e c$ is the Bohr magneton, c is the speed of light, and $\mathbf{s}$ is the spin operator. The single-particle confinement

$$U(r) = \frac{Ne^2}{2a^3}(r^2 - 3a^2)\Theta(a - r) - \frac{Ne^2}{r}\Theta(r - a) \qquad (2)$$

is harmonic with the Mie frequency $\omega_M = \sqrt{Ne^2/m_e a^3}$ inside the particle and Coulomb-like outside. In Eq. (2), $\Theta(x)$ denotes the Heaviside step function.

Assuming that the magnetic field points in the z direction, $\mathbf{B} = B\mathbf{e}_z$ (see Fig. 1), we can express the Hamiltonian (1) in the symmetric gauge $\mathbf{A} = (-y, x, 0)B/2$ as

$$H = \sum_i \left[\frac{p_i^2}{2m_e} + U(r_i) + \frac{\omega_c}{2}(l_{z,i} + 2s_{z,i}) \right] + \sum_{i,j} \frac{e^2}{2|\mathbf{r}_i - \mathbf{r}_j|}, \qquad (3)$$

where $\omega_c = eB/m_e c$ is the cyclotron frequency and l_z and s_z are the z components of angular momentum and spin, respectively. Notice that in writing Eq. (3), we omitted the diamagnetic term $\sum_i m_e \omega_c^2 (x_i^2 + y_i^2)/8$, which is quadratic in the magnetic field and of the order of $Nm_e \omega_c^2 a^2$. As the Mie frequency typically lies in the optical range and $\hbar \omega_c/B = 0.12$ meV/T, we have $\omega_c \ll \omega_M$, even for the highest presently achievable static magnetic fields of several tens of teslas. Thus, the diamagnetic term represents a small correction to the single-particle confinement (2), which is proportional to $(\omega_c/\omega_M)^2$. In the sequel we work to first order in the small parameter ω_c/ω_M.

A. Separation into collective and relative coordinates

A monochromatic electric field of (complex) amplitude $\mathbf{E}_0$ and frequency ω can be used to excite the electronic system. In the long-wavelength limit, the coupling to such an electric field is described by the Hamiltonian

$$H_f = -e \sum_i \mathbf{r}_i \cdot \mathbf{E}_0 \, e^{i\omega t}. \qquad (4)$$

This field only couples to the electronic center of mass. Hence, it is appealing to decompose the Hamiltonian (3) by introducing the electronic center-of-mass coordinate $\mathbf{R} = \sum_i \mathbf{r}_i/N$ and its conjugate momentum $\mathbf{P} = \sum_i \mathbf{p}_i$.[24,26] The relative coordinates are denoted by $\mathbf{r}'_i = \mathbf{r}_i - \mathbf{R}$ and $\mathbf{p}'_i = \mathbf{p}_i - \mathbf{P}/N$. Introducing this new set of coordinates in Eq. (3) and assuming that the displacement of the center of mass is much smaller than the nanoparticle size ($|\mathbf{R}| \ll a$), we obtain the decomposition

$$H = H_{cm} + H_{rel} + H_c + H_Z, \qquad (5)$$

where H_{cm} and H_{rel} are the center-of-mass and relative-coordinate Hamiltonians, respectively, and H_c is the coupling between them. The Zeeman term

$$H_Z = \omega_c \sum_i s_{z,i} \qquad (6)$$

accounts for the spin degrees of freedom. The decomposition (5) is reminiscent of the well-studied case where the degree of freedom of interest (in our case, the electronic center of mass) is coupled to a large reservoir or environment (the relative coordinates).[27] The interaction with the reservoir leads to the dissipation of the collective coordinate energy. The number of degrees of freedom of the reservoir is proportional to the number of electrons in the nanoparticle, and thus, it is not very large. However, it has been shown[28,29] that such a reservoir is sufficient to constitute a well-defined environment for the collective excitation, provided the nanoparticle is not extremely small.

The center-of-mass Hamiltonian appearing in Eq. (5) can be decomposed in two parts as

$$H_{\text{cm}} = H_{\text{cm}}^{\parallel} + H_{\text{cm}}^{\perp}, \tag{7}$$

with the part depending on the collective coordinate Z parallel to the magnetic field

$$H_{\text{cm}}^{\parallel} = \frac{P_Z^2}{2M} + \frac{M\tilde{\omega}_{\text{M}}^2}{2} Z^2, \tag{8}$$

and the transverse component

$$H_{\text{cm}}^{\perp} = \frac{P_X^2 + P_Y^2}{2M} + \frac{M\tilde{\omega}_{\text{M}}^2}{2}(X^2 + Y^2) + \frac{\omega_c}{2} L_Z. \tag{9}$$

Here $M = Nm_e$ and $L_Z = X P_Y - Y P_X$. The frequency $\tilde{\omega}_{\text{M}} = \omega_{\text{M}}\sqrt{1 - N_{\text{out}}/N}$ is slightly redshifted as compared to the bare Mie frequency by the spill-out effect,[2–4,24] where N_{out} is the number of electrons outside the nanoparticle. In what follows, we approximate $\tilde{\omega}_{\text{M}}$ by ω_{M} for simplicity. The Hamiltonian for the relative coordinates reads

$$H_{\text{rel}} = \sum_i \left[\frac{p_i'^2}{2m_e} + U(r_i') + \frac{\omega_c}{2} l_{z,i}' \right] + \sum_{i,j} \frac{e^2}{2|\mathbf{r}_i' - \mathbf{r}_j'|}, \tag{10}$$

and the coupling Hamiltonian

$$H_c = \sum_i \mathbf{R} \cdot [\nabla U(r_i')]|_{\mathbf{R}=0}, \tag{11}$$

with $\mathbf{R} \cdot \nabla U(r) = m_e \omega_{\text{M}}^2 \mathbf{R} \cdot \mathbf{r} f(r)$ and

$$f(r) = \Theta(a - r) + \left(\frac{a}{r}\right)^3 \Theta(r - a). \tag{12}$$

The parallel part (8) of the center-of-mass Hamiltonian describes a harmonic oscillator which is independent of the magnetic field and whose classical motion is sketched in Fig. 1. Its lowest excitation corresponds to the usual surface plasmon.[23,24] In contrast, the transverse part (9) includes the effect of the magnetic field. The two associated collective modes are called surface magnetoplasmons. Their corresponding classical orbits are sketched in Fig. 1. Thus, an electric field which is polarized parallel to the magnetic field will excite only the usual surface plasmon in the z direction. In contrast, when $\mathbf{E}_0 \perp \mathbf{B}$, only the surface magnetoplasmons will be excited. In the general case, when $\mathbf{E}_0$ has components perpendicular and parallel to $\mathbf{B}$, both the surface plasmon and the surface magnetoplasmons will be excited. Therefore, the relative orientation of the laser polarization and the external magnetic field allow one to selectively excite the different collective modes.

The Hamiltonian (9) is similar to the one encountered in the context of quasi-two-dimensional semiconductor quantum dots.[14,15] The main difference is that, unlike Eq. (2), the single-particle confinement in quantum dots is well approximated by a harmonic potential for all relevant r. Hence, due to Kohn's theorem,[14,15,30] center-of-mass and relative coordinates decouple. In metallic nanoparticles, the Coulomb tail of the single-particle confinement (2) leads to a non-negligible coupling Hamiltonian (11) and therefore to the decay of the surface (magneto)plasmon excitations. Another difference is that, in quasi-two-dimensional semiconductor quantum dots,

the relatively small effective electronic mass renders the cyclotron frequency of the order of the confining one, such that the diamagnetic term in the Hamiltonian (1) cannot be omitted in the context of quantum dots.

B. Effect of the magnetic field on the center-of-mass oscillation

The Hamiltonian (8) can be written as

$$H_{\text{cm}}^{\parallel} = \hbar\omega_{\text{M}}\left(b^{\dagger}b + \tfrac{1}{2}\right) \tag{13}$$

in terms of the bosonic operators

$$b = \frac{1}{\sqrt{2}}\left(\frac{Z}{\ell_{\text{osc}}} + i\frac{P_Z \ell_{\text{osc}}}{\hbar}\right), \tag{14a}$$

$$b^{\dagger} = \frac{1}{\sqrt{2}}\left(\frac{Z}{\ell_{\text{osc}}} - i\frac{P_Z \ell_{\text{osc}}}{\hbar}\right), \tag{14b}$$

with $\ell_{\text{osc}} = \sqrt{\hbar/M\omega_{\text{M}}}$ being the oscillator length.

The Hamiltonian $H_{\text{cm}}^{\perp}$ of Eq. (9) can be diagonalized by means of Fock-Darwin states.[14] Introducing the new variable $\xi = (X + iY)/\sqrt{2}$ and its complex conjugate and the bosonic operators

$$b_+ = \frac{1}{\sqrt{2}}\left(\frac{\xi^*}{\ell_{\text{osc}}} + \ell_{\text{osc}}\frac{\partial}{\partial\xi}\right), \tag{15a}$$

$$b_+^{\dagger} = \frac{1}{\sqrt{2}}\left(\frac{\xi}{\ell_{\text{osc}}} - \ell_{\text{osc}}\frac{\partial}{\partial\xi^*}\right), \tag{15b}$$

$$b_- = \frac{1}{\sqrt{2}}\left(\frac{\xi}{\ell_{\text{osc}}} + \ell_{\text{osc}}\frac{\partial}{\partial\xi^*}\right), \tag{15c}$$

$$b_-^{\dagger} = \frac{1}{\sqrt{2}}\left(\frac{\xi^*}{\ell_{\text{osc}}} - \ell_{\text{osc}}\frac{\partial}{\partial\xi}\right), \tag{15d}$$

we can write

$$H_{\text{cm}}^{\perp} = \hbar\omega_+\left(b_+^{\dagger}b_+ + \tfrac{1}{2}\right) + \hbar\omega_-\left(b_-^{\dagger}b_- + \tfrac{1}{2}\right). \tag{16}$$

The frequencies of the two magnetoplasmon excitations read[14]

$$\omega_{\pm} = \omega_{\text{M}} \pm \frac{\omega_c}{2}. \tag{17}$$

The surface magnetoplasmon with the larger (smaller) frequency ω_+ (ω_-) rotates counterclockwise (clockwise) in the plane perpendicular to the magnetic field (see Fig. 1). Notice that one has $\omega_+ > \omega_-$ since the Lorentz force $-Ne\dot{\mathbf{R}} \times \mathbf{B}$ increases (decreases) the strength of the confinement seen by the collective mode with frequency ω_+ (ω_-).

As is well known,[14,15] the effect of the magnetic field is thus to split the usual surface plasmon in the plane perpendicular to the field axis in two surface magnetoplasmon excitations whose frequencies are separated by the cyclotron frequency ω_c. However, the experimental observation of the two surface magnetoplasmon modes will be limited by the linewidths of these collective excitations. We address this important issue in Sec. III.

C. Mean-field approximation for the environment

The Hamiltonian for the relative coordinates (10) contains the electron-electron interactions. Assuming that the full correlations are not crucial for the present problem, we treat the interactions on a mean-field level. Numerical calculations using the local density approximation and performed in the

absence of a magnetic field[23] suggest that the self-consistent potential treating the interactions on a mean-field level can be approximated by

$$V(r) = V_0 \Theta(r - a), \tag{18}$$

a spherical square well of depth $V_0 = \varepsilon_F + W$, where ε_F and W are the Fermi energy and the work function of the considered nanoparticle, respectively. We expect that the square well shape of the effective potential remains a good approximation for $\omega_c \ll \omega_M$.[31] We thus write, at mean-field level,

$$H_{\text{rel}} = \sum_i \left[\frac{p_i'^2}{2m_e} + V(r_i') + \frac{\omega_c}{2} l_{z,i}' \right]. \tag{19}$$

In what follows, we rewrite the above Hamiltonian together with the Zeeman Hamiltonian (6) in second-quantized form,[32]

$$H_{\text{rel}} + H_Z = \sum_{\alpha\sigma} \varepsilon_{\alpha\sigma} c_{\alpha\sigma}^\dagger c_{\alpha\sigma}, \tag{20}$$

where the operators $c_{\alpha\sigma}^\dagger$ ($c_{\alpha\sigma}$) create (annihilate) one-body eigenstates $|\alpha, \sigma\rangle$ with eigenenergies $\varepsilon_{\alpha\sigma} = \varepsilon_\alpha - \sigma\hbar\omega_c/2$ in the mean-field potential $V(r)$. Here α is a shorthand notation for the orbital quantum numbers $(n_\alpha, l_\alpha, m_\alpha)$, with n_α, l_α, and m_α being the principal, azimuthal, and magnetic quantum numbers, respectively, while $\sigma = +1 (-1)$ corresponds to spin up (down). It is important to realize that the Hamiltonians of Eqs. (19) and (20) do contain the electron-electron interactions (at mean-field level) and thus that our subsequent results concerning the surface magnetoplasmon lifetimes incorporate the crucial role played by the electronic interactions.

D. Coupling of the center of mass to the environment

Under our mean-field assumption presented in Sec. II C and using Eqs. (14) and (15), the coupling Hamiltonian (11) can be written as

$$H_c = m_e \omega_M^2 \frac{\ell_{\text{osc}}}{\sqrt{2}} \sum_{\alpha\beta\sigma} c_{\alpha\sigma}^\dagger c_{\beta\sigma} \big[d_{\alpha\beta}^\sigma (b^\dagger + b)$$
$$+ d_{\alpha\beta,+}^\sigma (b_-^\dagger + b_+) + d_{\alpha\beta,-}^\sigma (b_+^\dagger + b_-) \big] \tag{21}$$

with the matrix elements

$$d_{\alpha\beta}^\sigma = \langle \alpha, \sigma | z f(r) | \beta, \sigma \rangle, \tag{22a}$$

$$d_{\alpha\beta,\pm}^\sigma = \frac{1}{\sqrt{2}} \langle \alpha, \sigma | (x \pm iy) f(r) | \beta, \sigma \rangle, \tag{22b}$$

which contain the function $f(r)$ of Eq. (12). The spherical symmetry of the wave functions associated with the Hamiltonian (20) allows us to decompose the matrix elements (22) into angular and radial parts,

$$d_{\alpha\beta}^\sigma = \mathcal{A}_{l_\alpha, l_\beta}^{m_\alpha, m_\beta} \mathcal{R}(\varepsilon_{\alpha\sigma}, \varepsilon_{\beta\sigma}), \tag{23a}$$

$$d_{\alpha\beta,\pm}^\sigma = \mathcal{A}_{l_\alpha, l_\beta,\pm}^{m_\alpha, m_\beta} \mathcal{R}(\varepsilon_{\alpha\sigma}, \varepsilon_{\beta\sigma}). \tag{23b}$$

The angular parts can be expressed in terms of Wigner $3j$ symbols[33] as

$$\mathcal{A}_{l_\alpha, l_\beta}^{m_\alpha, m_\beta} = (-1)^{m_\alpha} \sqrt{(2l_\alpha + 1)(2l_\beta + 1)}$$
$$\times \begin{pmatrix} l_\alpha & l_\beta & 1 \\ 0 & 0 & 0 \end{pmatrix} \begin{pmatrix} l_\alpha & l_\beta & 1 \\ -m_\alpha & m_\beta & 0 \end{pmatrix}, \tag{24a}$$

$$\mathcal{A}_{l_\alpha, l_\beta,\pm}^{m_\alpha, m_\beta} = \mp(-1)^{m_\alpha} \sqrt{(2l_\alpha + 1)(2l_\beta + 1)}$$
$$\times \begin{pmatrix} l_\alpha & l_\beta & 1 \\ 0 & 0 & 0 \end{pmatrix} \begin{pmatrix} l_\alpha & l_\beta & 1 \\ -m_\alpha & m_\beta & \pm 1 \end{pmatrix}, \tag{24b}$$

with the selection rules $l_\alpha = l_\beta \pm 1$ for Eqs. (24) and $m_\alpha = m_\beta$ and $m_\alpha = m_\beta \pm 1$ for Eqs. (24a) and (24b), respectively. The radial matrix element can be approximated by[21]

$$\mathcal{R}(\varepsilon_{\alpha\sigma}, \varepsilon_{\beta\sigma}) = \frac{2\hbar^2}{m_e a} \frac{\sqrt{\varepsilon_{\alpha\sigma} \varepsilon_{\beta\sigma}}}{(\varepsilon_{\alpha\sigma} - \varepsilon_{\beta\sigma})^2}, \tag{25}$$

an expression that is obtained under the assumption of infinite confinement $V_0 \to \infty$ in Eq. (18).[34]

III. SURFACE MAGNETOPLASMON DECAY RATES

A. Landau damping of the surface magnetoplasmon collective modes

For nanoparticles having intermediate sizes of the order of a few nanometers, the Landau damping[3] is the dominating decay channel for the collective plasmon modes.[18] The surface (magneto)plasmons decay by producing particle-hole pairs in the electronic environment whose energies correspond to the ones of the collective excitations. Treating the coupling Hamiltonian (21) as a perturbation, the corresponding surface plasmon and surface magnetoplasmon decay rates, whose inverses yield the lifetimes of these collective excitations, can be obtained from Fermi's golden rule. Assuming zero temperature,[35] we have the decay rates[23,24]

$$\gamma = \frac{\pi}{\hbar} \left(m_e \ell_{\text{osc}} \omega_M^2 \right)^2 \sum_{ph\sigma} \left| d_{ph}^\sigma \right|^2 \delta(\hbar\omega_M - \varepsilon_{p\sigma} + \varepsilon_{h\sigma}) \tag{26}$$

$$\gamma_\pm = \frac{\pi}{\hbar} \left(m_e \ell_{\text{osc}} \omega_M^2 \right)^2 \sum_{ph\sigma} \left| d_{ph,\pm}^\sigma \right|^2 \delta(\hbar\omega_\pm - \varepsilon_{p\sigma} + \varepsilon_{h\sigma}) \tag{27}$$

for the surface plasmon and surface magnetoplasmons, respectively. Here p and h denote particle and hole states with energies $\varepsilon_{p\sigma} > \varepsilon_F$ and $\varepsilon_{h\sigma} < \varepsilon_F$.

Using the expressions (23) for the coupling matrix elements and the appropriate selection rules that are contained in Eq. (24), we obtain to first order in $\omega_c/\omega_M \ll 1$

$$\gamma = \frac{2\pi}{\hbar} \left(\frac{2\ell_{\text{osc}}}{a} \right)^2 F, \tag{28a}$$

$$\gamma_\pm = \frac{2\pi}{\hbar} \left(\frac{2\ell_{\text{osc}}}{a} \right)^2 \left(1 \mp \frac{2\omega_c}{\omega_M} \right) F_\pm, \tag{28b}$$

where

$$F = \int_{\max(\varepsilon_F, \hbar\omega_M)}^{\varepsilon_F + \hbar\omega_M} d\varepsilon \, \varepsilon (\varepsilon - \hbar\omega_M) \sum_{l,m} \varrho_{l,m}(\varepsilon)$$
$$\times \big[\left(\mathcal{A}_{l,l+1}^{m,m} \right)^2 \varrho_{l+1,m}(\varepsilon - \hbar\omega_M)$$
$$+ \left(\mathcal{A}_{l,l-1}^{m,m} \right)^2 \varrho_{l-1,m}(\varepsilon - \hbar\omega_M) \big], \tag{29a}$$

$$F_\pm = \int_{\max(\varepsilon_F, \hbar\omega_\pm)}^{\varepsilon_F + \hbar\omega_\pm} d\varepsilon \, \varepsilon (\varepsilon - \hbar\omega_\pm) \sum_{l,m} \varrho_{l,m}(\varepsilon)$$
$$\times \big[\left(\mathcal{A}_{l,l+1,\pm}^{m,m\mp 1} \right)^2 \varrho_{l+1,m\mp 1}(\varepsilon - \hbar\omega_\pm)$$
$$+ \left(\mathcal{A}_{l,l-1,\pm}^{m,m\mp 1} \right)^2 \varrho_{l-1,m\mp 1}(\varepsilon - \hbar\omega_\pm) \big]. \tag{29b}$$

Here $\varrho_{l,m}(\varepsilon)$ is the density of states for fixed angular momentum l and magnetic quantum number m.[22] For metals the Fermi wave vector $k_F \simeq 10$ nm^{-1}, such that $k_F a \gg 1$ for nanoparticles having a radius of more than a nanometer. Thus, we can resort to the semiclassical approximation[36,37] to evaluate the density of states. To leading order in $\hbar$, we have[23,38]

$$\varrho_{l,m}(\varepsilon) = \frac{\sqrt{2m_e a^2(\varepsilon - \hbar\omega_c m/2)/\hbar^2 - (l+1/2)^2}}{2\pi(\varepsilon - \hbar\omega_c m/2)}, \quad (30)$$

which allows us to evaluate Eq. (29) in the semiclassical limit (for details, see Appendix A), leading to

$$\gamma = \frac{3v_F}{4a}g(\nu) \quad (31)$$

for the surface plasmon decay rate. Here, v_F denotes the Fermi velocity, and $\nu = \hbar\omega_M/\varepsilon_F$. The function $g(\nu)$ given in Appendix B [cf. Eq. (B2)] is a monotonously decreasing function. It is remarkable that the result of Eq. (31), which has been obtained to first order in the small parameter ω_c/ω_M, does not present any magnetic field dependence. We can thus conclude that for realistic field strengths the surface plasmon is not influenced by the external magnetic field. The result of Eq. (31) and its well-known $1/a$ size dependence was first obtained by Kawabata and Kubo[19] and refined later by many authors.[4,20-24]

For the two surface magnetoplasmon collective modes, we find for $\omega_c \ll (\omega_M, \varepsilon_F/\hbar)$ (see Appendix A for details) the decay rates

$$\gamma_\pm = \frac{3v_F}{4a}\left[g(\nu) \mp \frac{\omega_c}{\omega_M}\left(\frac{3}{2}g(\nu) - \frac{\nu}{2}g'(\nu) - h(\nu)\right)\right], \quad (32)$$

which constitute the main results of our work. Here $g'(\nu)$ denotes the derivative of the function $g(\nu)$ given in Eq. (B2), and the function $h(\nu)$ is given in Appendix B [cf. Eq. (B4)]. The surface magnetoplasmon decay rates (32) present the same size dependence as that of the surface plasmon, Eq. (31), and obviously verify $\gamma_\pm = \gamma$ for zero magnetic field ($\omega_c = 0$). It is important to realize that the function $3g(\nu)/2 - \nu g'(\nu)/2 - h(\nu)$ entering the result of Eq. (32) is positive for $\nu \lesssim 4.51$, i.e., it is positive for any realistic values of the parameter $\nu = \hbar\omega_M/\varepsilon_F$. Thus, we conclude that γ_+ (γ_-) decreases (increases) linearly for increasing ω_c (i.e., increasing magnetic field). This is due to the fact that the frequency ω_+ (ω_-) of the corresponding mode shows the opposite behavior, i.e., it increases (decreases) with ω_c [cf. Eq. (17)]. The behavior of the decay rates $\gamma_\pm$ of Eq. (32) as a function of the magnetic field can easily be explained as follows: The typical dipole matrix elements between particle and hole states separated by an energy $\Delta\varepsilon_{ph} = \varepsilon_p - \varepsilon_h$ entering the Fermi golden rule (27) scale as $d^\sigma_{ph,\pm} \sim 1/\Delta\varepsilon^2_{ph}$, while the density of particle-hole states fulfilling the selection rules dictated by the angular part (24b) of the matrix elements $d^\sigma_{ph,\pm}$ is linear in $\Delta\varepsilon_{ph}$. Since energy conservation requires that $\Delta\varepsilon_{ph} = \hbar\omega_\pm$, this argument, valid in the limit $\hbar\omega_c \ll \hbar\omega_M \ll \varepsilon_F$ (for details, see Ref. 28), where $g(0) = 1$, $g'(0) = 0$, and $h(0) = 0$, yields the scaling $\gamma_\pm \sim 1/\omega^3_\pm \sim 1 \mp 3\omega_c/2\omega_M$, consistent with Eq. (32).

B. Extension to dielectric environments and noble-metal and ferromagnetic nanoparticles

In the case of alkali clusters in vacuum, the result of Eq. (31) for the surface plasmon decay rate agrees quantitatively with numerical calculations using the time-dependent local density approximation as well as with experiments. We take this as a strong indication that the surface magnetoplasmon decay rate (32) is quantitatively valid for alkaline clusters in a vacuum as well. When one considers alkaline nanoparticles in a dielectric environment or noble-metal nanoparticles (in vacuum or in an embedding matrix), one has to take into account the steepness of the effective mean-field potential $V(r)$ entering Eq. (19) in the derivation of Eq. (31) to get quantitative agreement with numerical calculations as well as with experiments.[23] The resulting linewidth of the surface plasmon excitation decreases as the dielectric constants of the metal and of the dielectric environment increase. This is also the case for the linewidths of the surface magnetoplasmons. Hence, their observation will be facilitated by a dielectric environment.

Furthermore, our results for the decay rates of the collective electronic excitations should, at least qualitatively, be applicable to ferromagnetic nanoparticles, provided one adds to the external magnetic field **B** the internal magnetic field $4\pi\mathbf{M}_s$,[13] with $\mathbf{M}_s$ being the saturation magnetization. This internal field couples to the orbital degrees of freedom and is of the order of 2T for bulk transition ferromagnets. Thus, in saturated ferromagnetic nanoparticles, the surface magnetoplasmons might exist even in the absence of an external magnetic field. This possible extension of our considerations toward ferromagnetic nanoparticles might be important for the analysis of the magnetization dynamics in such systems[9,12] since the surface magnetoplasmons create electromagnetic fields inside the particle that might affect the magnetic moments responsible for the magnetism in these nanoparticles.

IV. EXPERIMENTAL DETECTION OF SURFACE MAGNETOPLASMONS

A. Absorption profiles

For the nanoparticle radii of a few nanometer that we are considering, the extinction spectrum is dominated by absorption.[4,39] Assuming a Lorentzian profile for the line shapes of the collective modes, the (normalized) absorption cross section of photons with frequency ω is given by

$$\sigma_\parallel(\omega) = \frac{\gamma/2\pi}{(\omega - \omega_M)^2 + (\gamma/2)^2} \quad (33)$$

when the illuminating electric field is polarized parallel to the magnetic field [$\mathbf{E}_0 = E_0\mathbf{e}_z \parallel \mathbf{B}$, cf. Eq. (4)]. In that case, only the usual magnetic-field-independent surface plasmon is excited.

In the case where $\mathbf{E}_0 \perp \mathbf{B}$, the two collective surface magnetoplasmon modes are triggered. Using linearly polarized light with $\mathbf{E}_0 = E_0(\cos\varphi\,\mathbf{e}_x + \sin\varphi\,\mathbf{e}_y)$, both magnetoplasmons are excited, and the absorption cross section reads

$$\sigma_\perp(\omega) = \frac{1}{2}\left[\sigma_+(\omega) + \sigma_-(\omega)\right], \quad (34)$$

with

$$\sigma_+(\omega) = \frac{\gamma_+/2\pi}{(\omega - \omega_+)^2 + (\gamma_+/2)^2} \tag{35}$$

$$\sigma_-(\omega) = \frac{\gamma_-/2\pi}{(\omega - \omega_-)^2 + (\gamma_-/2)^2}. \tag{36}$$

The absorption profile $\sigma_\perp$, scaled with the maximum $2/\pi\gamma$ of $\sigma_\parallel$, is shown in Fig. 2 as a function of the photon frequency ω and for increasing cyclotron frequency ω_c for the case of a sodium nanoparticle of radius $a = 10$ nm having a collective surface plasmon resonance at $\hbar\omega_M = 3.5\text{eV}$. In the regime of currently available static magnetic fields, up to about 40T (horizontal white solid line in Fig. 2), the two magnetoplasmon modes (indicated by black lines in Fig. 2) are separated by a frequency ω_c which is smaller than the surface magnetoplasmon linewidths γ_+ and γ_- [Eq. (32)]. These linewidths are of the same order as that of the surface plasmon γ [Eq. (31)].[40] Hence, the linewidths are larger than the separation of the resonances such that the two modes may not be directly resolved in an absorption spectrum.[41] It should be noted that even using pulsed magnetic fields that can reach up to 70T would not allow us to clearly separate the two modes. As can be seen from Fig. 2, only for unrealistically large $\omega_c/\omega_M \gtrsim$ 1% do the two collective excitations exhibit separate maxima.

A way to individually address the surface magnetoplasmons is to use circularly polarized light. In the case where $\mathbf{E}_0 = E_0(\mathbf{e}_x + i\mathbf{e}_y)/\sqrt{2}$ $[\mathbf{E}_0 = E_0(\mathbf{e}_x - i\mathbf{e}_y)/\sqrt{2}]$, one can selectively excite the surface magnetoplasmon with frequency ω_+ $[\omega_-]$, and the absorption spectrum is given by Eq. (35) [Eq. (36)]. But for currently experimentally achievable magnetic fields, the displacement in frequency, as well as the
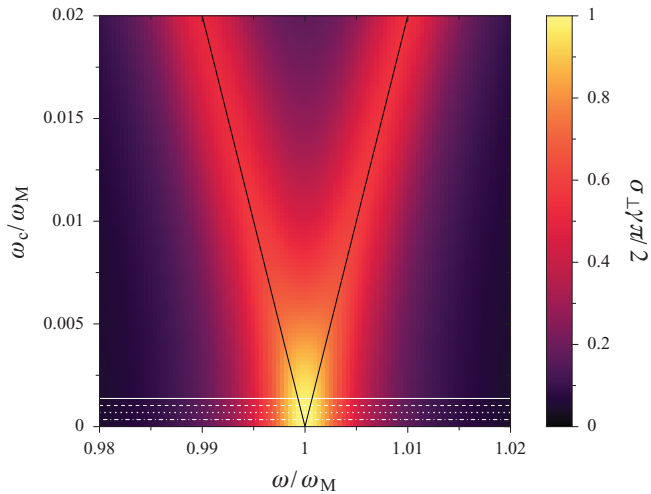

FIG. 2. (Color online) Absorption cross section $\sigma_\perp$ for linearly polarized light with electric field perpendicular to the external magnetic field [Eq. (34)] as a function of the photon frequency ω and the cyclotron frequency ω_c, both scaled with the Mie frequency ω_M. The chosen parameters correspond to a sodium nanoparticle ($r_s = 3.93a_0$, where a_0 is the Bohr radius) of radius $a = 10$ nm, having $\hbar\omega_M = 3.5$ eV. The horizontal white lines correspond to magnetic fields $B = 10$T (dash-dotted line), $B = 20$T (dotted line), $B = 30$T (dashed line), and $B = 40$T (solid line). The black lines indicate the surface magnetoplasmon resonance frequencies, ω_- (left line) and ω_+ (right line) [see Eq. (17)].

modification of the linewidth of these peaks, is so small that it might not be observable.

In addition, for an ensemble of nanoparticles, the inhomogeneous broadening due to their dispersion in size further increases the total linewidth. Thus, the direct and unambiguous observation of two distinct resolved peaks in the absorption spectrum of an ensemble of nanoparticles using linearly polarized light might not be possible. Moreover, using circularly polarized light which enables us to excite a single surface magnetoplasmon mode may not present a sufficient magnetic-field-dependent behavior in the absorption cross section. However, we suggest in the following two differential measurements where one could experimentally identify the effect of the magnetic field on the collective excitations and the presence of the surface magnetoplasmons, one using linearly polarized light (Sec. IV B) and the other, which is more efficient, using circularly polarized light (Sec. IV C). The effect of inhomogeneous broadening on these proposed differential measurements is discussed in Sec. IV D.

B. Detection with linearly polarized light

The relative differential absorption cross section

$$\frac{\Delta\sigma_{\text{lin}}}{\sigma} = \frac{\sigma_\parallel - \sigma_\perp}{\sigma_\parallel} \tag{37}$$

given by the difference between the absorption cross sections for the electric field linearly polarized parallel [Eq. (33)] and perpendicular [Eq. (34)] to the external magnetic field is depicted in Fig. 3 for the values of the magnetic field indicated by the white lines in Fig. 2 (the parameters are for the same sodium nanoparticles of radius $a = 10$ nm). It can be seen in Fig. 3 that the differential absorption $\Delta\sigma_{\text{lin}}/\sigma$ increases for increasing magnetic field strength, yielding a clear signature of the existence of the surface magnetoplasmon excitations. The increase of the total linewidth of the absorption resonance caused by the magnetic field via the modified width and the splitting of the surface magnetoplasmons leads to positive values of $\Delta\sigma_{\text{lin}}/\sigma$ in the center of the resonance and to negative values in the tails. In magnetic fields of less than 10T, $\Delta\sigma_{\text{lin}}/\sigma$ is very small, at least for the case of sodium nanoparticles. However, in a field of 40T (solid lines in Figs. 2 and 3), of the
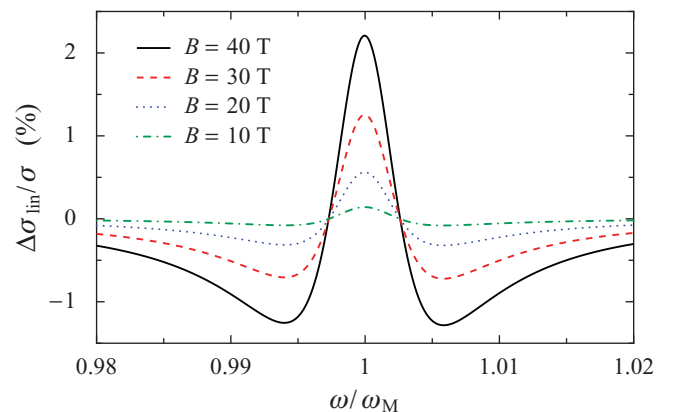

FIG. 3. (Color online) Differential absorption cross section $\Delta\sigma_{\text{lin}}/\sigma$ of Eq. (37) as a function of the photon frequency ω. The parameters are the same as in Fig. 2. The values of the magnetic field used in this figure correspond to the horizontal white lines in Fig. 2.

order of the highest static field available in present-day high magnetic field laboratories, the differential absorption $\Delta\sigma_{lin}/\sigma$ becomes noticeable. Furthermore, magnetic field pulses of 70T are available with durations of the order of milliseconds that should be sufficient to measure the absorption cross section. For the latter value, we expect a relative differential absorption of about 6% that should be detectable (not shown in Fig. 3).

C. Detection with circularly polarized light

The relative differential absorption cross section

$$\frac{\Delta\sigma_{cir}}{\sigma} = \frac{\sigma_+ - \sigma_-}{\sigma_+ + \sigma_-} \qquad (38)$$

given by the difference between absorption cross sections for the two circular polarizations of the electric field, Eqs. (35) and (36), is shown in Fig. 4 for the same parameters as in Figs. 2 and 3. It is positive (negative) for $\omega > \omega_M$ ($\omega < \omega_M$) due to the fact that the resonance frequency ω_+ (ω_-) of the surface magnetoplasmon mode "+" ("−") is larger (smaller) than the surface plasmon frequency ω_M [cf. Eq. (17)]. As one can see from Fig. 4, the differential absorption cross section $\Delta\sigma_{cir}/\Delta\sigma$ of Eq. (38) is much more pronounced than the one of Eq. (37) using linearly polarized light (compare with Fig. 3). Moreover, the frequency range where $\Delta\sigma_{cir}/\sigma$ presents noticeable values is much broader. In the case of circularly polarized light, $\Delta\sigma_{cir}/\sigma$ is already of the order of several percent at a magnetic field of 10T (green dash-dotted line in Fig. 4) and can reach up to about 15% in a static field of 40T (black solid line). For a pulsed magnetic field of 70T, we obtain a maximal relative differential cross section of about 25% (not shown in the figure). It thus seems even more efficient to use circularly polarized light rather than linearly polarized light to detect the surface magnetoplasmon modes in metallic nanoparticles.

D. Effect of inhomogeneous broadening

In Secs. IV A, IV B, and IV C, we have implicitly assumed that the nanoparticles irradiated by the laser light do not present any size dispersion. Although this is a valid approximation for experiments on single clusters,[42–47] most experiments are done on ensembles of metallic clusters where the inhomogeneous
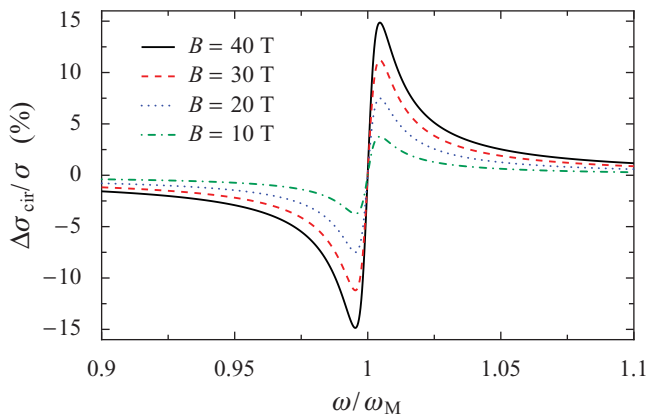
broadening resulting from the size dependence of the resonance frequency masks the homogeneous linewidth.[48–50]

In this section, we address the role of inhomogeneous broadening on the experimental detection of the two surface magnetoplasmon excitations. To this end, in the absorption cross sections of Eqs. (33), (35), and (36), we phenomenologically add an inhomogeneous linewidth γ_{in} resulting from the size dispersion of the ensemble of nanoparticles to the intrinsic linewidths of the surface (magneto)plasmon collective modes. The resulting differential absorption cross sections for sodium nanoparticles with mean radius $\bar{a} = 10$ nm in a magnetic field of 10T using circularly polarized light [cf. Eq. (38)] are presented in Fig. 5. Results for the same parameters using linearly polarized light [cf. Eq. (37)] are shown in the inset in Fig. 5.

We quantify the inhomogeneous broadening γ_{in} by its relative value with respect to the intrinsic linewidth of the collective modes at zero magnetic field, γ [see Eq. (31)]. Given the size dependence of the resonance frequency of the surface plasmon excitation which can be estimated from numerical calculations within the time-dependent local density approximation (see Fig. 7 in Ref. 24) and assuming a constant size distribution with dispersion Δa around the mean radius $\bar{a}$, we find that $\Delta a/\bar{a} = 50\%$ ($\Delta a/\bar{a} = 100\%$) corresponds to $\gamma_{in}/\gamma = 0.5$ ($\gamma_{in}/\gamma = 1$) for the parameters of Fig. 5 (see blue dotted and red dashed lines).

As one can see from Fig. 5, inhomogeneous broadening tends to weaken the differential absorption cross sections. Indeed, the maxima of the differential cross sections for circularly (Fig. 5) and linearly polarized light (inset in Fig. 5) decrease for increasing inhomogeneous linewidth γ_{in}. For an inhomogeneous linewidth γ_{in} comparable to the intrinsic linewidth γ, the maximal differential absorption cross section using circularly polarized light, $\Delta\sigma_{cir}/\sigma$, is still of about 2% in a magnetic field of 10T (see red dashed line in Fig. 5). Such $\Delta\sigma_{cir}/\sigma$ should still be clearly measurable.[49,50] In the case of linearly polarized light, the maximal differential absorption cross section is only about 0.03% for $\gamma_{in} = \gamma$ (see red dashed line in the inset in Fig. 5). Such a small value in the difference
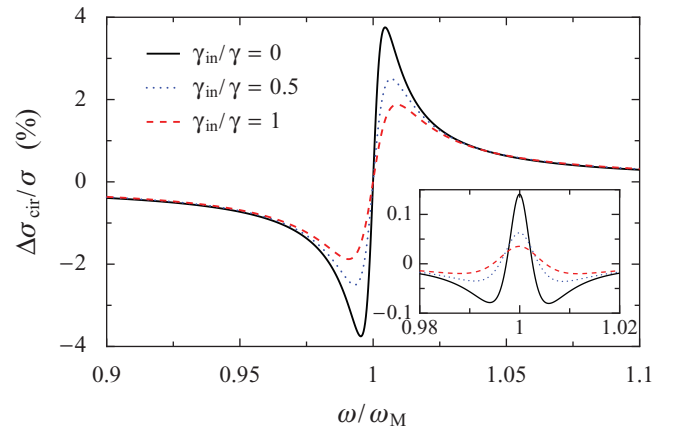

FIG. 4. (Color online) Differential absorption cross section $\Delta\sigma_{cir}/\sigma$ of Eq. (38) as a function of the photon frequency ω. The parameters are the same as in Figs. 2 and 3.

FIG. 5. (Color online) Differential absorption cross section $\Delta\sigma_{cir}/\sigma$ of Eq. (38) as a function of the photon frequency ω in a magnetic field $B = 10$T for an ensemble of sodium nanoparticles with mean radius $\bar{a} = 10$nm and for increasing values of the inhomogeneous linewidth γ_{in}. The inset is the same as the main figure for linearly polarized light, Eq. (37).

between two extinction spectra on ensembles of nanoparticles seems to be difficult to measure.[49,50] These results point out that using circularly polarized light to obtain a clear-cut experimental detection of the two surface magnetoplasmon excitations in ensembles of metallic nanoparticles presenting a rather large size (and shape) dispersion is more appropriate than using linearly polarized light.

V. CONCLUSION

We have analyzed the role of an external magnetic field on collective excitations in metallic nanoparticles. As is the case in the context of semiconductor quantum dots, the magnetic field induces two new resonances in metallic nanoparticles, the surface magnetoplasmons, which can be excited when the polarization of the electric field has a component perpendicular to the magnetic field. Our main result concerns the Landau damping linewidths of these collective modes that we have calculated. In particular, we have shown treating the electron-electron interactions within a mean-field approximation how the magnetic field modifies the absorption linewidths of the surface magnetoplasmon resonances. In all realistic cases, the linewidths are much larger than the splitting of the resonance energies such that one may not resolve them directly in a single absorption measurement. Nevertheless, if one changes the polarization of the electric field with respect to the magnetic field from parallel to perpendicular, a noticeable change in the absorption profiles should be detectable, at least in very strong magnetic fields, as they are currently available in high-field laboratories. Using circularly polarized light, which enables one to selectively excite the surface magnetoplasmon modes, leads to even larger values of the differential cross section when one changes the polarization from right-handed to left-handed. The proposed differential measurements are expected to allow a detection of the surface magnetoplasmon modes even in the presence of an inhomogeneous broadening of the resonances that results from the size and shape dispersion for ensembles of nanoparticles in matrices.

Our results can be extended to ferromagnetic nanoparticles, where the internal magnetic field (i.e., the saturation magnetization) couples to the orbital degrees of freedom. In addition, when the ground-state magnetization in nanoparticles is nonzero, the collective electronic excitations couple to spin-dependent excitations in the nanoparticle.[51] This is the case in nanoparticles with an open electronic shell, particularly for the case of ferromagnetic nanoparticles. It then becomes possible to affect the magnetization indirectly by exciting the charge degrees of freedom, and the influence of the magnetic field on the latter might become important.

APPENDIX A: SEMICLASSICAL CALCULATION OF THE SURFACE PLASMON AND SURFACE MAGNETOPLASMON LINEWIDTHS

In this Appendix, we present the details of our semiclassical calculation of the surface (magneto)plasmon linewidths discussed in Sec. III A. Introducing the notation $\varepsilon_0 = \hbar^2/2m_e a^2$ and $\kappa = \hbar\omega_c/2\varepsilon_0$, we expand the semiclassical density of states for fixed l and m [Eq. (30)] for $\varepsilon \gg \hbar\omega_c$ to obtain[52]

$$\varrho_{l,m}(\varepsilon) \simeq \varrho_{l,0}(\varepsilon)\left[1 + \kappa m f_l(\varepsilon)\right], \tag{A1}$$

where

$$f_l(\varepsilon) = \frac{1}{\varepsilon/\varepsilon_0} - \frac{1}{2}\frac{1}{\varepsilon/\varepsilon_0 - (l+1/2)^2}. \tag{A2}$$

With Eq. (A1) and using the expression of the angular matrix elements (24), the functions F and $F_\pm$ [cf. Eq. (29)] that enter the surface plasmon and surface magnetoplasmon linewidths [cf. Eq. (28)] read

$$F = \frac{1}{3}\int_{\max(\varepsilon_F,\hbar\omega_M)}^{\varepsilon_F+\hbar\omega_M} d\varepsilon\, \varepsilon(\varepsilon - \hbar\omega_M)\sum_l \varrho_{l,0}(\varepsilon)[(l+1)\varrho_{l+1,0}(\varepsilon - \hbar\omega_M) + l\varrho_{l-1,0}(\varepsilon - \hbar\omega_M)], \tag{A3a}$$

$$F_\pm = \frac{1}{3}\int_{\max(\varepsilon_F,\hbar\omega_\pm)}^{\varepsilon_F+\hbar\omega_\pm} d\varepsilon\, \varepsilon(\varepsilon - \hbar\omega_\pm)\sum_l \varrho_{l,0}(\varepsilon)\Bigg\{(l+1)\varrho_{l+1,0}(\varepsilon - \hbar\omega_\pm)\Bigg[1 \mp \kappa f_{l+1}(\varepsilon - \hbar\omega_\pm) \mp \frac{l}{2}\kappa(f_l(\varepsilon - \hbar\omega_\pm)$$

$$+ f_{l+1}(\varepsilon - \hbar\omega_\pm))\Bigg] + l\varrho_{l-1,0}(\varepsilon - \hbar\omega_\pm)\Bigg[1 \mp \kappa f_{l-1}(\varepsilon - \hbar\omega_\pm) \pm \frac{l+1}{2}\kappa(f_l(\varepsilon - \hbar\omega_\pm) + f_{l-1}(\varepsilon - \hbar\omega_\pm))\Bigg]\Bigg\}. \tag{A3b}$$

Consistently with the semiclassical approximation (high-energy limit), we now assume that $l \gg 1$ (i.e., $l \simeq l \pm 1$) and approximate in Eq. (A3) the summation over l by an integral. With Eqs. (30) and (A2), we obtain

$$F = \frac{1}{3(2\pi)^2}\int_{\max(\varepsilon_F,\hbar\omega_M)}^{\varepsilon_F+\hbar\omega_M} d\varepsilon \int_0^{\sqrt{(\varepsilon - \hbar\omega_M)/\varepsilon_0}} dl\, 2l\sqrt{\left(\frac{\varepsilon}{\varepsilon_0} - l^2\right)\left(\frac{\varepsilon - \hbar\omega_M}{\varepsilon_0} - l^2\right)}, \tag{A4a}$$

$$F_\pm = \frac{1}{3(2\pi)^2}\int_{\max(\varepsilon_F,\hbar\omega_\pm)}^{\varepsilon_F+\hbar\omega_\pm} d\varepsilon \int_0^{\sqrt{(\varepsilon - \hbar\omega_\pm)/\varepsilon_0}} dl\, 2l\sqrt{\left(\frac{\varepsilon}{\varepsilon_0} - l^2\right)\left(\frac{\varepsilon - \hbar\omega_\pm}{\varepsilon_0} - l^2\right)}\left\{1 \pm \kappa\left[\frac{1}{2}\frac{1}{(\varepsilon - \hbar\omega_\pm)/\varepsilon_0 - l^2} - \frac{\varepsilon_0}{\varepsilon - \hbar\omega_\pm}\right]\right\}. \tag{A4b}$$

Expanding the above expressions for $\omega_c \ll \omega_M$, one finds with Eq. (28) our final results for the surface (magneto)plasmon linewidths, Eqs. (31) and (32).

APPENDIX B: AUXILIARY FUNCTIONS FOR THE SURFACE PLASMON AND SURFACE MAGNETOPLASMON LINEWIDTHS

The function $g(\nu)$ entering the surface plasmon linewidth (31) is defined as

$$g(\nu) = \frac{2}{\nu} \int_{\max(1,\nu)}^{1+\nu} dx \int_0^{x-\nu} dy \sqrt{(x-y)(x-y-\nu)}. \quad \text{(B1)}$$

The double integral can easily be evaluated, and one finds[21]

$$g(\nu) = \frac{1}{3\nu}\left[(1+\nu)^{3/2} - (1-\nu)^{3/2}\right]$$
$$+ \frac{\nu}{4}(\sqrt{1+\nu} - \sqrt{1-\nu} - \nu \ln \nu)$$
$$+ \frac{\nu}{2}\left[\left(1+\frac{\nu}{2}\right)\ln(\sqrt{1+\nu}-1)\right.$$
$$\left. - \left(1-\frac{\nu}{2}\right)\ln(1-\sqrt{1-\nu})\right] \quad \text{(B2a)}$$

for $\nu \leqslant 1$ and

$$g(\nu) = \frac{1}{3\nu}(1+\nu)^{3/2} + \frac{\nu}{4}(\sqrt{1+\nu} - \ln\nu)$$
$$+ \frac{\nu}{2}\left[\left(1+\frac{\nu}{2}\right)\ln(\sqrt{1+\nu}-1) - \frac{\nu}{2}\ln\sqrt{\nu}\right] \quad \text{(B2b)}$$
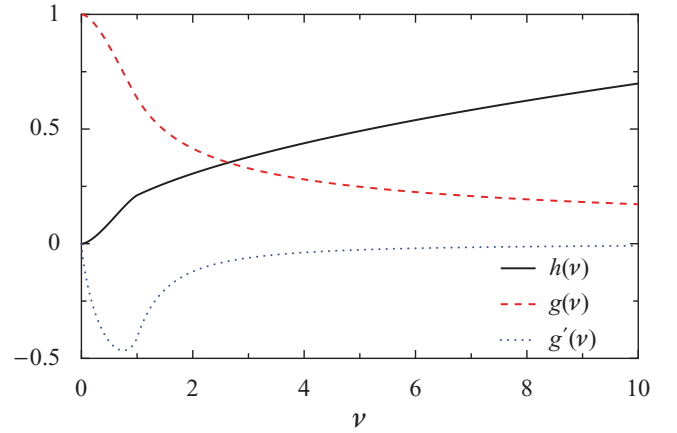

FIG. 6. (Color online) The function $g(\nu)$ of Eq. (B2) (red dashed line), its derivative $g'(\nu)$ (blue dotted line), and the function $h(\nu)$ of Eq. (B4) (black solid line).

for $\nu > 1$. The function $g(\nu)$ is shown in Fig. 6 (red dashed line). Its asymptotic behaviors are $g(\nu) \simeq 1 + \nu^2[\ln(\nu/4) - 1/6]/4$ and $g(\nu) \simeq 8/15\sqrt{\nu}$ for $\nu \ll 1$ and $\nu \gg 1$, respectively. Its derivative $g'(\nu)$ entering the surface magnetoplasmon linewidth (32) is shown as a blue dotted line.

The function $h(\nu)$ entering the surface magnetoplasmon linewidths (32) is defined as

$$h(\nu) = \int_{\max(1,\nu)}^{1+\nu} dx \int_0^{x-\nu} dy \sqrt{(x-y)(x-y-\nu)}$$
$$\times \left[\frac{1}{2(x-y-\nu)} - \frac{1}{x-\nu}\right]. \quad \text{(B3)}$$

Its explicit expression reads

$$h(\nu) = -\frac{\nu}{2}\left\{\sqrt{1+\nu} - \sqrt{1-\nu} + \ln\left(\frac{\sqrt{1+\nu}-1}{\sqrt{\nu}}\right)\left[1 - \frac{\nu}{2}\ln\left(\frac{\sqrt{1+\nu}-1}{\sqrt{\nu}}\right)\right]\right.$$
$$- \ln\left(\frac{1-\sqrt{1-\nu}}{\sqrt{\nu}}\right)\left[1 - \nu - \frac{\nu}{2}\ln\left(\frac{1-\sqrt{1-\nu}}{\sqrt{\nu}}\right)\right] + \nu\left[\ln\left(\frac{\sqrt{1+\nu}-1}{\sqrt{\nu}}\right)\ln\left(\frac{\sqrt{1+\nu}-1+\sqrt{\nu}}{\sqrt{\nu}}\right)\right.$$
$$- \ln\left(\frac{1-\sqrt{1-\nu}}{\sqrt{\nu}}\right)\ln\left(\frac{1-\sqrt{1-\nu}+\sqrt{\nu}}{\sqrt{\nu}}\right) + \text{Li}_2\left(\frac{1-\sqrt{1+\nu}}{\sqrt{\nu}}\right) - \text{Li}_2\left(\frac{\sqrt{\nu}+1-\sqrt{1+\nu}}{\sqrt{\nu}}\right)$$
$$\left.\left. - \text{Li}_2\left(\frac{\sqrt{1-\nu}-1}{\sqrt{\nu}}\right) + \text{Li}_2\left(\frac{\sqrt{\nu}+\sqrt{1-\nu}-1}{\sqrt{\nu}}\right)\right]\right\} \quad \text{(B4a)}$$

for $\nu \leqslant 1$ and

$$h(\nu) = -\frac{\nu}{2}\left\{\sqrt{1+\nu} + \ln\left(\frac{\sqrt{1+\nu}-1}{\sqrt{\nu}}\right)\left[1 - \frac{\nu}{2}\ln\left(\frac{\sqrt{1+\nu}-1}{\sqrt{\nu}}\right)\right] + \nu\left[\ln\left(\frac{\sqrt{1+\nu}-1}{\sqrt{\nu}}\right)\ln\left(\frac{\sqrt{1+\nu}-1+\sqrt{\nu}}{\sqrt{\nu}}\right)\right.\right.$$
$$\left.\left. + \text{Li}_2\left(\frac{1-\sqrt{1+\nu}}{\sqrt{\nu}}\right) - \text{Li}_2\left(\frac{\sqrt{\nu}+1-\sqrt{1+\nu}}{\sqrt{\nu}}\right) + \frac{\pi^2}{12}\right]\right\} \quad \text{(B4b)}$$

for $\nu > 1$. It involves the dilogarithmic function

$$\text{Li}_2(z) = \sum_{k=1}^{\infty} \frac{z^k}{k^2} = \int_z^0 dt\, \frac{\ln(1-t)}{t}. \quad \text{(B5)}$$

The asymptotic behaviors of the function $h(\nu)$ for $\nu \ll 1$ and $\nu \gg 1$ read $h(\nu) \simeq -\nu^2[\ln(\nu/4)+1]/4$ and $h(\nu) \simeq 2\sqrt{\nu}/9$, respectively. The function $h(\nu)$ is plotted in Fig. 6 (black solid line).

[1] W. A. de Heer, Rev. Mod. Phys. **65**, 611(1993).

[2] M. Brack, Rev. Mod. Phys. **65**, 677(1993).

[3] G. F. Bertsch and R. A. Broglia, *Oscillations in Finite Quantum Systems* (Cambridge University Press, Cambridge, 1994).

[4] U. Kreibig and M. Vollmer, *Optical Properties of Metal Clusters* (Springer-Verlag, Berlin, 1995).

[5] J.-Y. Bigot, J.-C. Merle, O. Cregut, and A. Daunois, Phys. Rev. Lett. **75**, 4702 (1995).

[6] J.-Y. Bigot, V. Halté, J.-C. Merle, and A. Daunois, Chem. Phys. **251**, 181 (2000).

[7] N. Del Fatti, F. Vallée, C. Flytzanis, Y. Hamanaka, and A. Nakamura, Chem. Phys. **251**, 215 (2000).

[8] G. Weick, D. Weinmann, G.-L. Ingold, and R. A. Jalabert, EPL **78**, 27002 (2007).

[9] L. H. F. Andrade, A. Laraoui, M. Vomir, D. Muller, J.-P. Stoquert, C. Estournès, E. Beaurepaire, and J.-Y. Bigot, Phys. Rev. Lett. **97**, 127401 (2006).

[10] M. Vomir, L. H. F. Andrade, L. Guidoni, E. Beaurepaire, and J.-Y. Bigot, Phys. Rev. Lett. **94**, 237601 (2005).

[11] J.-Y. Bigot, M. Vomir, and E. Beaurepaire, Nat. Phys. **5**, 515 (2009), and references therein.

[12] A. Kirilyuk, A. V. Kimel, and T. Rasing, Rev. Mod. Phys. **82**, 2731 (2010).

[13] C. Kittel, Phys. Rev. Lett. **10**, 339 (1963).

[14] L. Jacak, P. Hawrylak, and A. Wójs, *Quantum Dots* (Springer-Verlag, Berlin, 1998).

[15] S. M. Reimann and M. Manninen, Rev. Mod. Phys. **74**, 1283 (2002).

[16] Ch. Sikorski and U. Merkt, Phys. Rev. Lett. **62**, 2164 (1989).

[17] B. Meurer, D. Heitmann, and K. Ploog, Phys. Rev. Lett. **68**, 1371 (1992).

[18] For nanoparticle radii $a \gtrsim 10$ nm, the radiation damping dominates over the Landau damping. The corresponding lifetime decreases as the volume of the nanoparticle increases as $1/a^3$ (see, e.g., Ref. 4).

[19] A. Kawabata and R. Kubo, J. Phys. Soc. Jpn. **21**, 1765 (1966).

[20] M. Barma and V. Subrahmanyam, J. Phys. Condens. Matter **1**, 7681 (1989).

[21] C. Yannouleas and R. A. Broglia, Ann. Phys. (NY) **217**, 105 (1992).

[22] R. A. Molina, D. Weinmann, and R. A. Jalabert, Phys. Rev. B **65**, 155427 (2002).

[23] G. Weick, R. A. Molina, D. Weinmann, and R. A. Jalabert, Phys. Rev. B **72**, 115410 (2005).

[24] G. Weick, G.-L. Ingold, R. A. Jalabert, and D. Weinmann, Phys. Rev. B **74**, 165421 (2006).

[25] Throughout the paper, we use cgs units.

[26] L. G. Gerchikov, C. Guet, and A. N. Ipatov, Phys. Rev. A **66**, 053202 (2002).

[27] U. Weiss, *Quantum Dissipative Systems* (World Scientific, Singapore, 1993).

[28] C. Seoanez, G. Weick, R. A. Jalabert, and D. Weinmann, Eur. Phys. J. D **44**, 351 (2007).

[29] G. Weick, G.-L. Ingold, D. Weinmann, and R. A. Jalabert, Eur. Phys. J. D **44**, 359 (2007).

[30] W. Kohn, Phys. Rev. **123**, 1242 (1961).

[31] K. Tanaka, S. C. Creagh, and M. Brack, Phys. Rev. B **53**, 16050 (1996).

[32] We assume here that the number of valence electrons is large ($N \gg 1$), such that $N - 1 \simeq N$. Therefore, the number of relative degrees of freedom equals the total one.

[33] A. R. Edmonds, *Angular Momentum in Quantum Mechanics* (Princeton University Press, Princeton, NJ, 1960).

[34] This approximation is well justified for nanometer-sized particles: The evanescent part of a wave function of energy $\varepsilon < V_0$ can be neglected when $\sqrt{2m(V_0 - \varepsilon)}a/\hbar \gg 1$. In typical nanoparticles one has $V_0 - \varepsilon \simeq \varepsilon_{\rm F}$ such that $V_0 \to \infty$ becomes allowed when $k_{\rm F} a \gg 1$, with $k_{\rm F}$ being the Fermi wave vector. This is fulfilled since $k_{\rm F} \simeq 10$ nm^{-1} for metals.

[35] The electronic temperature T of the system is much smaller than the Fermi temperature $T_{\rm F}$, which is of the order of 10^4 to 10^5 K for typical metals. Thus, the effect of temperature on the surface (magneto)plasmon linewidths can be neglected here. For its effect in the case of the usual surface plasmon linewidth, where finite-temperature corrections are of order $(T/T_{\rm F})^2$, see Ref. 24. The temperature correction for the surface magnetoplasmon linewidths [see Eq. (32)] is expected to be the same.

[36] M. C. Gutzwiller, *Chaos in Classical and Quantum Mechanics* (Springer-Verlag, Berlin, 1990).

[37] M. Brack and R. K. Bhaduri, *Semiclassical Physics*, Frontiers in Physics, Vol. 96 (Addison-Wesley, Reading, MA, 1997).

[38] Higher-order corrections in $\hbar$ to the density of states lead to an oscillation of the surface plasmon lifetime as a function of the size of the nanoparticle (Refs. 22 and 23). This effect is only relevant for very small nanoparticles ($a \lesssim 1.5$ nm), and we disregard it here.

[39] M. Born and E. Wolf, *Principles of Optics* (Cambridge University Press, Cambridge, 1999).

[40] For the parameters of Fig. 2, $\hbar\gamma = 32$ meV.

[41] The $1/a$ size dependence of the decay rates (32) suggests that taking larger nanoparticles would facilitate the observation of two well-defined surface magnetoplasmon lines in the absorption spectrum. However, for large nanoparticles ($a \gtrsim 10$ nm), the radiation damping decay rate $\gamma_{\rm rad} \propto a^3$ increases above the Landau damping (Ref. 4) and masks the two collective resonances.

[42] T. Klar, M. Perner, S. Grosse, G. von Plessen, W. Spirkl, and J. Feldmann, Phys. Rev. Lett. **80**, 4249 (1998).

[43] C. Sönnichsen, T. Franzl, T. Wilk, G. von Plessen, and J. Feldmann, New J. Phys. **4**, 93 (2002).

[44] A. Arbouet, D. Christofilos, N. Del Fatti, F. Vallée, J. R. Huntzinger, L. Arnaud, P. Billaud, and M. Broyer, Phys. Rev. Lett. **93**, 127401 (2004).

[45] S. Berciaud, L. Cognet, G. A. Blab, and B. Lounis, Phys. Rev. Lett. **93**, 257402 (2004).

[46] S. Berciaud, L. Cognet, P. Tamarat, and B. Lounis, Nano Lett. **5**, 515 (2005).

[47] M. A. van Dijk, M. Lippitz, and M. Orrit, Phys. Rev. Lett. **95**, 267406 (2005).

[48] B. Lamprecht, J. R. Krenn, A. Leiner, and F. R. Aussenegg, Appl. Phys. B **69**, 223 (1999).

[49] F. Stietz, J. Bosbach, T. Wenzel, T. Vartanyan, A. Goldmann, and F. Träger, Phys. Rev. Lett. **84**, 5644 (2000).

[50] J. Bosbach, C. Hendrich, F. Stietz, T. Vartanyan, and F. Träger, Phys. Rev. Lett. **89**, 257404 (2002).

[51] Y. Yin, P.-A. Hervieux, R. A. Jalabert, G. Manfredi, E. Maurat, and D. Weinmann, Phys. Rev. B **80**, 115416 (2009).

[52] The total density of states $\varrho(\varepsilon) = \sum_{lm} \varrho_{l,m}(\varepsilon)$ corresponds to the leading order Weyl term of the classical density of states (Ref. 23) and is thus independent of the magnetic field (Refs. 53 and 31).

[53] K. Richter, D. Ullmo, and R. A. Jalabert, Phys. Rep. **276**, 1 (1996).